Occurrence of Extreme Precipitation Events in California and Relationships with the Madden–Julian Oscillation

CHARLES JONES

Institute for Computational Earth System Science (ICESS), University of California, Santa Barbara, Santa Barbara, California

(Manuscript received 18 October 1999, in final form 1 February 2000)

ABSTRACT

California receives most of the annual precipitation during the boreal winter season. Additionally, large spatial and temporal variations in the total rainfall amounts are observed. This study investigates the occurrence of extreme precipitation events in California and the modulation by the Madden–Julian oscillation (MJO). Three questions are investigated. 1) Are extreme precipitation events in California more likely to occur during active MJO than inactive periods? 2) In what phase of the MJO life cycle are extreme events more likely? 3) Are interannual variations in the frequency of extreme events in California related to interannual variations of the MJO?

Daily totals derived from gridded hourly station data are used to define extreme precipitation events from January 1958 to December 1996. Outgoing longwave radiation from polar orbiting satellites (1979–96) and zonal component of the wind at 200 hPa and 850 hPa from the National Centers for Environmental Prediction–National Center for Atmospheric Research reanalysis (1958–96) are used to describe the life cycle of the oscillation and its interannual variability. The results indicate that the frequency of extreme events are more common when tropical activity associated with the MJO is high, as opposed to periods of quiescent phases of the oscillation. Second, a slight preference for a higher number of events is observed when convective anomalies are located in the Indian Ocean. In this situation, low-level westerly and easterly wind anomalies are observed over the Indian and western Pacific Oceans, respectively. The analysis of the interannual variability in the amplitude of the MJO and the occurrence of extreme events over California indicates no direct and systematic relationships with the number of extreme events.

1. Introduction

The climatology of the state of California shows that the bulk of the annual precipitation occurs during the boreal winter season (Bryson and Hare 1974; Raphael and Mills 1996; Higgins et al. 1999). Additionally, large spatial variations in the total rainfall amounts are observed; for example, in a typical winter season northern California can receive 2 to 4 times more precipitation than the southern part of the state. However and most importantly, significant temporal variations are also observed in rainfall extending from synoptic to intraseasonal, interannual, decadal, and longer timescales.

On interannual timescales, the El Niño–Southern Oscillation (ENSO) is the strongest signal of large-scale variations in the ocean–atmosphere system (Horel and Wallace 1981; Philander 1990). Several studies have investigated a possible relationship between El Niño occurrence and changes in California rainfall, although not all the studies reach the same conclusions. While a few studies indicate some modulation in the California rainfall by ENSO, other investigations find no clear association (Schonher and Nicholson 1989; Mitchell and Blier 1997). It appears that since ENSO episodes have varying characteristics in spatial structure, intensity, and duration, different ENSO events may impact precipitation over the state of California differently (Null 1993).

This study is concerned with the influence of tropical intraseasonal variations on precipitation in California. The Madden–Julian oscillation (MJO) is the main mode of large-scale tropical intraseasonal variability with an important role in the climate system (Madden and Julian 1994; Meehl et al. 1996; Jones et al. 1998, 1999). On this timescale, intraseasonal variations seem to be extremely important to wintertime rainfall in California as well (Mo and Higgins 1998a). Higgins and Mo (1997) developed a composite study to identify possible relationships between Persistent North Pacific (PNP) circulation anomalies and tropical intraseasonal variations. They found that remote forcing from the Tropics seems to play a significant role in the development of PNP

Corresponding author address: Dr. Charles Jones, Institute for Computational Earth System Science (ICESS), University of California, Santa Barbara, CA 93106-3060.
E-mail: cjones@icess.ucsb.edu

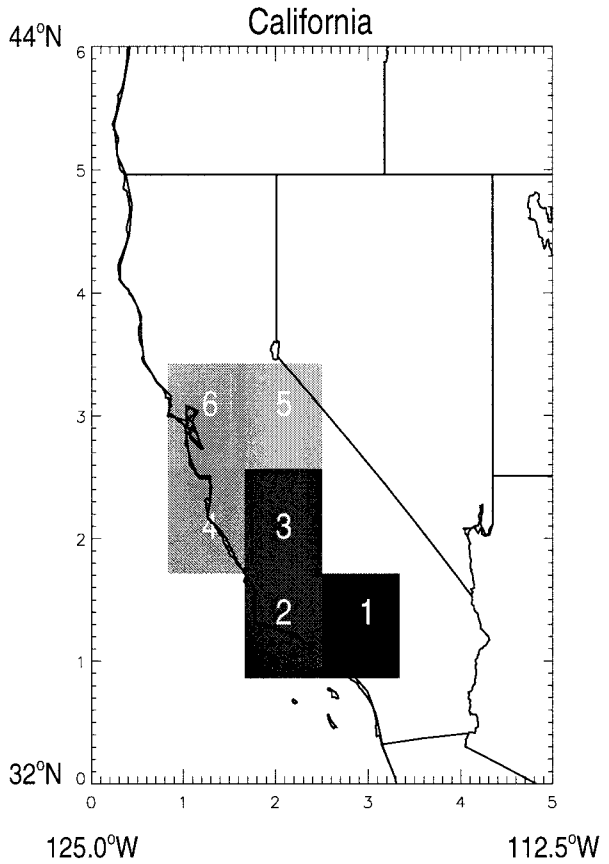

FIG. 1. Selection of the six grid boxes in the state of California from which precipitation extremes are investigated. The dimensions of the boxes are 2° lat. × 2.5° long.

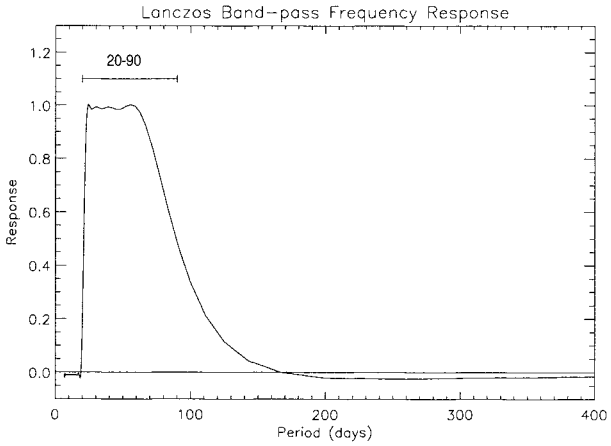

FIG. 2. Frequency response of a Lanczos bandpass filter with 49 weights and cutoff frequency responses of 20 and 90 days^{-1}.

prior to onset. Tropical heat sources generate subtropical Rossby wave vorticity anomalies that are partially responsible for the retraction (extension) of the Pacific jet stream exit region and the formation of PNP anomalies. Their results are also consistent with the study of Higgins and Schubert (1996) who analyzed simulations from a general circulation model and found that tropical intraseasonal heat variations are phase locked with the development of PNP anomalies. In a more recent study, Mo and Higgins (1998a,b) further investigated linkages between atmospheric circulation anomalies and hydrological processes associated with California. Their results show additional evidence that the MJO modulates California precipitation. Wet (dry) events are favored during the phase of the oscillation associated with enhanced convection near 150°E (120°E) in the tropical Pacific.

Previous studies have shown linkages between intraseasonal tropical–extratropical interactions and weather variations in the western coast of North America. This has important implications for prediction purposes, since very wet or very dry seasons, have profound impacts with attendant serious social and economic consequences. For instance, a high frequency of extreme precipitation events can lead to saturated soil moisture conditions and increased runoff that oftentimes is accompanied by severe floods. Motivated by these reasons, this study investigates three questions. First, are extreme precipitation events in California more likely to occur during active MJO than inactive periods? Second, in what phase of the MJO life cycle are extreme events more likely? Third, the MJO is also known to exhibit large interannual amplitudes (Weickmann 1991). Therefore, are interannual variations in the frequency

TABLE 1. Annual average precipitation (mm) (1 Jan 1958–31 Dec 1996) and statistics of extreme events in precipitation over California. Values are computed over the six grid boxes. The thresholds T_5, T_{10}, and T_{15} are 5%, 10%, and 15% values of the annual average precipitation. These thresholds correspond approximately to 90th, 95th, and 97th percentiles, respectively. The total number of 5-day precipitation totals exceeding the T_5, T_{10}, and T_{15} thresholds are also indicated. These values are computed for the hydrological calendar defined as 20–24 Jul from one year to 15–19 Jul of the succeeding year.

	Box 1	Box 2	Box 3	Box 4	Box 5	Box 6
Annual average precipitation (mm)	379.26	397.25	386.05	436.00	795.37	666.13
5% Threshold (T_5)(mm)	18.96	19.86	19.30	21.80	39.77	33.31
10% Threshold (T_{10})(mm)	37.93	39.73	38.61	43.60	79.54	66.61
15% Threshold (T_{15})(mm)	56.89	59.59	57.91	65.40	119.30	99.92
Number of type-I events	230	228	245	266	258	276
Number of type-II events	113	113	85	82	66	71
Number of type-III events	62	56	41	29	24	17

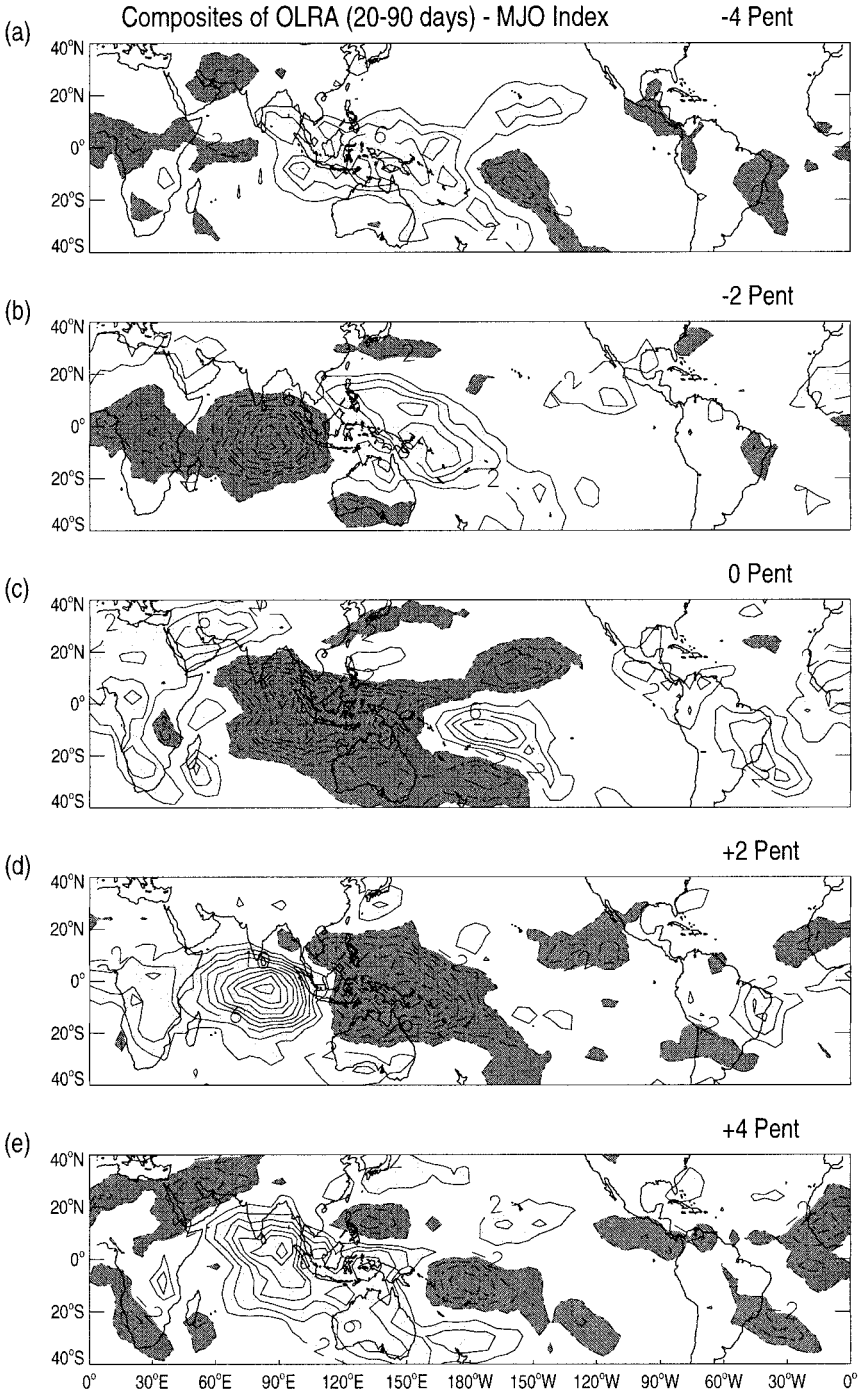

FIG. 3. Lag composites of OLR anomalies in the 20–90-day band. Composites are computed for periods when the amplitude of the OLR index (see text for details) is negative and less than minus one standard deviation. Lags are from −4 to +4 pentads. The lag composites are denoted as active MJO cases. The sample size for each composite is 181 pentads in the period 1979–96. Dark (light) shadings indicate OLR anomalies less (greater) than −2 W m^{-2} (+2 W m^{-2}). Contour interval is 2 W m^{-2}.

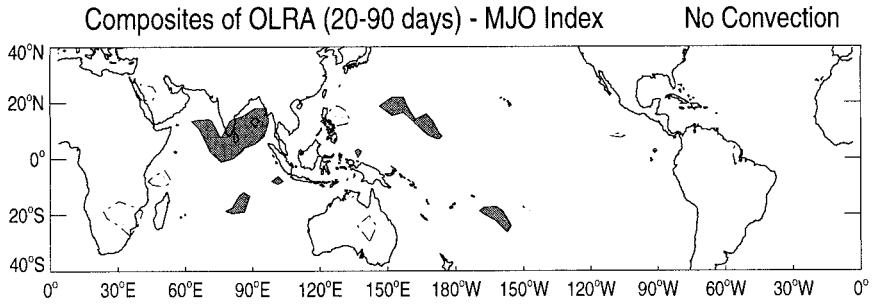

FIG. 4. Composite of OLR anomalies in the 20–90-day band. Composite is computed for periods when the amplitude of the OLR index (see text for details) is negative but greater than −0.3 standard deviation. This case is denoted as inactive MJO cases. The sample size for each composite is 166 pentads in the period 1979–96. Dark (light) shadings indicate OLR anomalies less (greater) than −2 W m^{-2} (+2 W m^{-2}). Contour interval is 2 W m^{-2}.

of extreme events in California related to interannual variations of the MJO?

The paper is organized as follows. We first describe the datasets used in this study (section 2) and then discuss the definition of extreme precipitation events used throughout this work (section 3). We next address the first two questions discussed above, that is, whether or not extreme events are more likely when the MJO is active (section 4). The relationships between interannual variations in extreme events in California and the MJO are discussed in section 5. Our discussion and conclusions are presented in section 6.

2. Data

The precipitation used in this study is the daily totals derived from gridded hourly station data, which were kindly provided by Higgins et al. (1996). The daily totals are displayed on 2° latitude by 2.5° longitude grid covering the continental United States. The data record analyzed here extends from 1 January 1958 to 31 December 1996. Only 54 days out of 14 246 days are missing. Based on the daily precipitation, 5-day nonoverlapping totals were constructed for the period above. This resulted in time series with 2847 data points, of which eight 5-day totals were missing. The 5-day totals are used because this study focuses on extreme events that might be related to low-frequency tropical intraseasonal variations.

The life cycle of the MJO is characterized in this study in terms of variations in tropical convection and zonal component of the wind, specifically those that occur at the intraseasonal timescale. To describe variations in tropical convection, we use outgoing longwave radiation (OLR) data, which has been frequently used as a proxy for large-scale tropical convective activity (e.g., Lau and Chan 1986; Waliser et al. 1993; Jones et al. 1998). Pentads of OLR (5-day nonoverlapping means with 73 pentads per year; total of 1314 pentads) were obtained from the National Centers for Environmental Prediction (NCEP) from 1–5 January 1979 to 27–31 December 1996. Additional information on changes in instrumentation, equator-crossing times, and inherent biases in the OLR data can be found in Chelliah and Arkin (1992) and Waliser and Zhou (1997). Since the record of OLR only extends to 18 years, the MJO is also described with variations in the zonal component of the wind at 200 hPa (U200) and 850 hPa (U850). The NCEP–National Center for Atmospheric Research (NCAR) reanalysis (Kalnay et al. 1996) were used to define pentads of U200 and U850 for the 39-yr record from 1–5 January 1958 to 27–31 December 1996 (total of 2847 pentads).

3. Extreme precipitation events in California

In order to investigate possible linkages between extreme precipitation events and the activity of the MJO, we have selected six grid boxes over the state of California (Fig. 1). This selection focuses in the central and southern parts of the state. Although more grid boxes could have been chosen, we limit our analysis to this selection since each grid box is analyzed separately and therefore this makes the display and discussion of the results more manageable. In addition, we are particularly interested in extreme events along the coastal regions in the southern part of the state, since severe floods often accompany these extreme events.

Different definitions of what characterizes an extreme event in precipitation have been proposed in the literature (Dole and Gordon 1983; Mo and Higgins 1998a; Cayan et al. 1999). Extreme events in this study are defined as follows. For each of the six grid boxes, we computed the annual mean precipitation from 1958 to 1996. An extreme event of type I occurs if the 5-day total precipitation amount exceeds 5% of the annual mean. Similarly, we define extreme events of type II and type III if the 5-day total precipitation exceeds 10% and 15% of the annual mean, respectively. The extreme events defined as above correspond approximately to the 90th, 95th, and 97.5th percentiles, respectively. Table 1 summarizes the annual mean precipitation (mm),

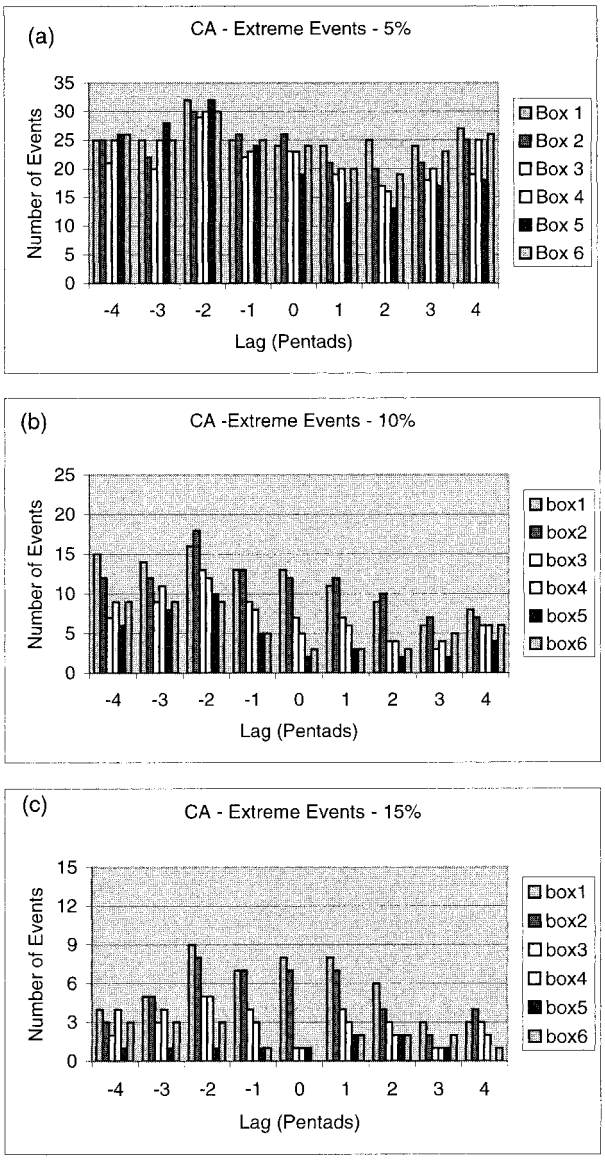

FIG. 5. Total number of extreme events in each of the six grid boxes shown in Fig. 1. The number of occurrences is counted for each lag of the OLR composites illustrated in Fig. 3. Horizontal axes indicate the time lag in pentads. The number of occurrences is counted for extreme events of (a) type I, (b) type II, and (c) type III.

5%, 10%, and 15% thresholds and the total number of extreme events in each grid box for the entire data record. Note that the annual mean precipitation increases from Box 1 to Box 6. Type-I extreme events are common in all six grid boxes and range from 230 to 276 in the period 1958–96. In contrast, extreme events of type II and type III are more frequent in southern California than in the central region. This is somewhat expected, since the wet and dry seasons are much more accentuated in the southern part of the state. The definition of three types of extreme events (weak, moderate, and severe) also allows assessing the sensitivity of the statistical results discussed next.

4. Extreme events in California and the Madden–Julian oscillation

The relationships between extreme events in precipitation and the MJO are now examined in detail. To obtain intraseasonal anomalies and characterize the MJO, a Lanczos bandpass filter with 49 weights and cutoff frequency responses of 0.5 at 20 and 90 days^{-1} was applied to the OLR, U200 and U850 pentads (Duchon 1979; Jones et al. 1998). The frequency response of this filter is shown in Fig. 2. This bandwidth is chosen to specifically resolve tropical intraseasonal variations associated with the MJO. In the remainder of this section, we investigate the hypothesis that extreme events in California are more frequent during active phases of the MJO.

a. Occurrences related to outgoing long wave radiation anomalies

The life cycle of the MJO is first examined with respect to variations in the OLR field. We have computed an empirical orthogonal function (EOF) analysis of the OLR anomalies (20–90 days) for the period 1–5 May 1979 through 3–7 September 1996 (total of 1266 pentads). Several previous studies have shown that the first two eigenvectors are separated from the remaining ones and together they describe the propagating behavior of the oscillation (Ferranti et al. 1990; Jones and Weare 1996). Based on the first two time coefficients (or principal components) derived from the EOF analysis of OLR anomalies (OLRA), we constructed an index based on the linear combination given by

$$\mathrm{OLRA}(t) = \mathrm{PC1}(t) + [\mathrm{PC2}(t+2) + \mathrm{PC2}(t+3)]/2. \quad (1)$$

The linear combination involves a time lag for PC2, since PC1 leads PC2 by 2 to 3 pentads. Similar index using anomalies of U at 850 hPa has been proposed by Maloney and Hartmann (1998) in their composite study of the life cycle of the MJO. They further demonstrated that the index for U850 effectively captures the large-scale structure of the MJO. The results are insensitive whether one uses PC1 and PC2 individually or with the linear combination above.

In order to test the hypothesis that extreme events are more frequent during active phases of the MJO, we further selected periods according to the amplitude of the OLRA index (1). Two cases were selected. First, situations of strong convective activity anomalies related to the MJO were chosen when the amplitude of the OLRA index is negative and less than minus one standard deviation. We refer to this case simply as the active MJO period. A second case was selected, referred

TABLE 2. Distribution of the number of 5%, 10%, and 15% extreme events for cases of strong convective anomalies associated with the MJO (OLRA index at lag −2), (sample size $n_1 = 181$ pentads) and no organized convection due to the MJO (sample size $n_2 = 166$ pentads). The value of the Z statistic for each case and box is also indicated. The Z values greater than $Z_{95} = 1.64$ indicate that the difference between the two proportions is significant at 95% confidence level.

	Type-I extreme events (5%)		Type-II extreme events (10%)		Type-III extreme events (15%)	
	Tropical MJO convection (lag −2)	No tropical MJO convection	Tropical MJO convection (lag −2)	No tropical MJO convection	Tropical MJO convection (lag −2)	No tropical MJO convection
Box 1	32	17	16	10	9	5
	$Z = 1.988$		$Z = 1.033$		$Z = 0.980$	
Box 2	30	16	18	12	8	7
	$Z = 1.913$		$Z = 0.927$		$Z = 0.098$	
Box 3	29	16	13	9	5	4
	$Z = 1.780$		$Z = 0.702$		$Z = 0.220$	
Box 4	30	20	12	9	5	5
	$Z = 1.197$		$Z = 0.493$		$Z = -0.148$	
Box 5	32	22	10	5	1	3
	$Z = 1.127$		$Z = 1.214$		$Z = -1.173$	
Box 6	30	22	9	9	3	5
	$Z = 0.862$		$Z = -0.198$		$Z = -0.896$	

to as the inactive MJO, so that the amplitude of the OLRA index is negative but greater than −0.3 standard deviation. A total of 181 and 166 pentads were selected for the active and inactive MJO cases, respectively. The lag composite of OLR anomalies for the active MJO cases, Fig. 3, shows the typical eastward-propagating behavior of the MJO in the convection field. In contrast, the average of all inactive cases, Fig. 4, shows, as expected, very weak OLR anomalies in the tropical belt. Thus, these choices of thresholds for active and inactive MJO ensures that the sample sizes are approximately equal as well as characterize very different situations of tropical intraseasonal variability. Note that selecting positive amplitudes of the OLRA index simply change the phases of the lag composites.

The next step consisted in counting the total number of extreme events of types I, II, and III during active MJO cases for each grid box and lag (Fig. 5). For type I (Fig. 5a), an average of about 23 extreme events occurs in all grid boxes and lags. There is, however, a slight tendency for more extreme events at lag −2 pentads (about 30 events), which corresponds to the situation when convective anomalies are intense over the Indian Ocean (cf. Fig. 3). Likewise, there are less extreme events at lag +2 pentads when convective anomalies are located between 120° and 150°E. The number of type-II extreme events for each lag and box (Fig. 5b) also shows some preference for more occurrences at negative lags. An average of eight type-II events for all lags and boxes are observed, although the variability among boxes and lags is quite large. As the threshold increases, type-III events (Fig. 5c), the number of extreme cases decreases. There is still, however, some preference for more events at lags −2 to +1 pentads, especially in southern California (grid boxes 1 and 2). The number of type-III extreme events is quite low in grid boxes 5 and 6.

We compare now the occurrence of extreme events during active MJO with inactive periods. The number of extreme events during the inactive MJO periods (Fig. 4) was also counted for each of the six grid boxes. The discussion is presented by contrasting the occurrences of types-I, -II, and -III events during situations of enhanced MJO convection at lag −2 pentads with the frequency of occurrence of inactive MJO convection. Table 2 summarizes the total counts. It is interesting to note that for types I and II (5% and 10%, respectively) there is usually a higher frequency of occurrence during enhanced MJO convection. In contrast, the same is not observed for the severe type-III events.

In order to determine whether or not such differences are statistically significant, we performed the following test. Extreme events of types I, II, and III are considered binomial variables in the sense that any given 5-day period either exceeds the 5%, 10%, or 15% thresholds or not. Next, we computed the test statistic Z for each type of extreme event and grid box defined as

$$Z = \frac{P_1 - P_2}{\sqrt{PQ(1/N_1 + 1/N_2)}}. \tag{2}$$

In this expression, P_1 and P_2 are the estimated probabilities of occurrence of extreme events for the active and inactive MJO situations, respectively. The standard error of the difference between the two proportions is given by the denominator. Here, P and Q are the common probabilities of occurrence and nonoccurrence of extreme events, and N_1 (181 pentads) and N_2 (166 pentads) are the sample sizes of the active and inactive MJO periods. The null hypothesis is H_0: $P_1 \leq P_2$ and the alternative is H_1: $P_1 > P_2$. The null hypothesis is rejected if the sample proportion P_1 is much greater than the sample proportion P_2 (see Anderson and Finn 1996, pp. 477–481). The value of the Z statistic is also shown in Table 2 for each type of extreme event and grid box. Values of Z greater than 1.64 indicate that the differences between the proportions are statistically significant at 95% level. Note, however, that this statistical

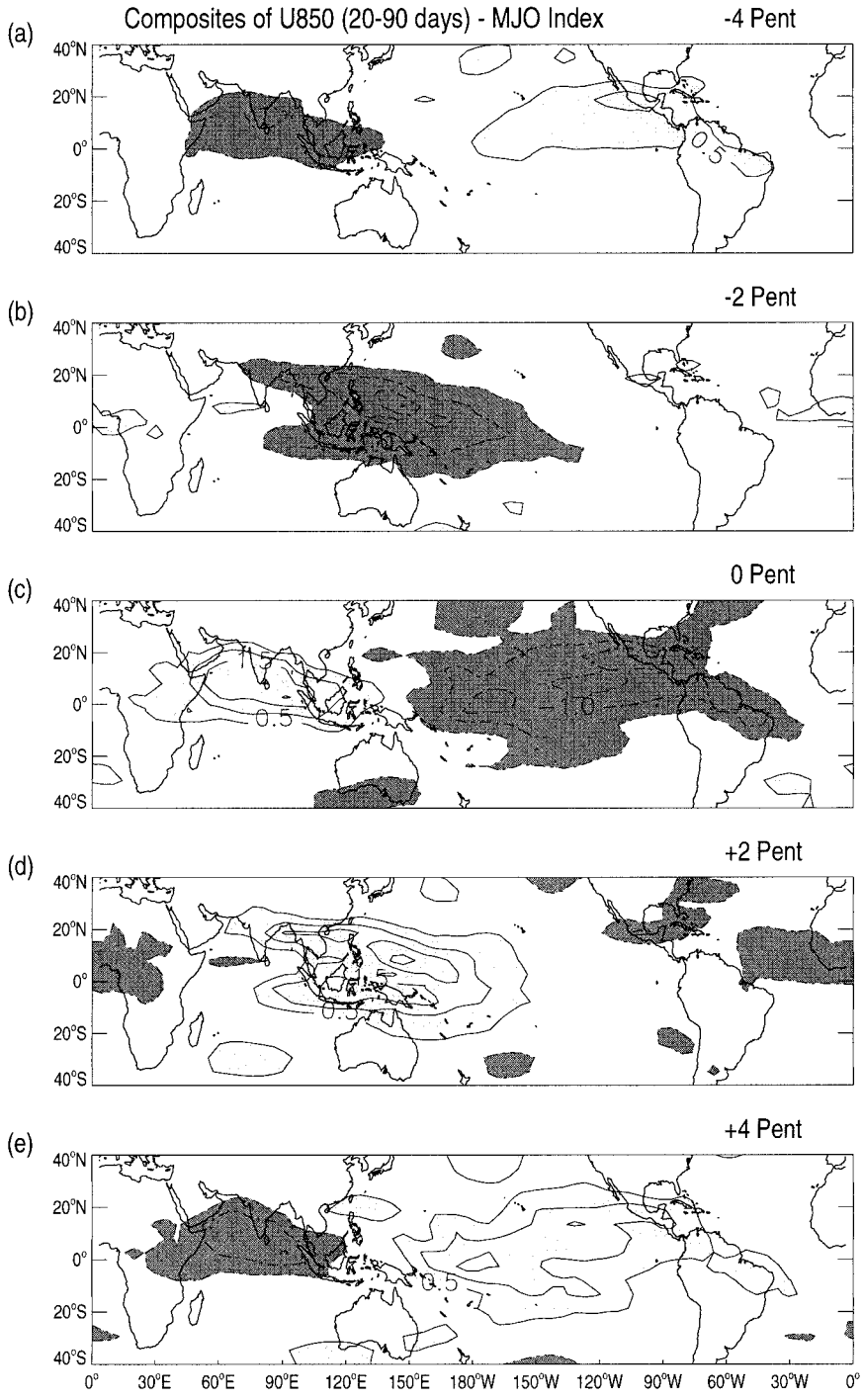

FIG. 6. Lag composites of 20–90-day anomalies in the zonal component of the wind at 850 hPa (U850). Composites are computed for periods when the amplitude of the U850 index (see text for details) is negative and less than minus one standard deviation. Lags are from −4 to +4 pentads. The lag composites are denoted as active MJO cases. The sample size for each composite is 439 pentads in the period 1958–96. Dark (light) shadings indicate U850 anomalies less (greater) than −0.5 m s^{-1} (+0.5 m s^{-1}). Contour interval is 0.5 m s^{-1}.

test does not account for possible serial correlation between pentads, that is, the occurrence (or nonoccurrence) of event in a given pentad may not necessarily be independent of occurrence (or nonocurrence) in adjacent pentads. Although there are always more type-I and -II events during the active MJO phases, the differences are statistically significant only for grid boxes 1, 2, and 3 and type-I event. However, as it will be discussed next, the difference between active and inactive MJO are considerably more significant when a dynamical field representative of the MJO cycle is used.

b. Occurrences related to zonal wind anomalies

The life cycle of the MJO is also represented by variations in the zonal component of the wind at 850 hPa. This has the advantage of the much longer data record based on the NCEP–NCAR reanalysis (1958–96). The approach follows the one described by Maloney and Hartmann (1998). An EOF analysis of U850 anomalies (20–90 days) in the equatorial belt 10°S–10°N was performed and the time coefficients (PC1 and PC2) associated with the first two leading EOFs were linearly combined to produce an index given by

$$\mathrm{U850}(t) = \mathrm{PC1}(t) + [\mathrm{PC2}(t + 2) + \mathrm{PC2}(t + 3)]/2. \quad (3)$$

Active MJO periods were selected when the amplitude of the U850 index is negative and less than minus one standard deviation. This resulted in a sample size of 439 pentads. Periods of inactive MJO were selected when the U850 index is negative but greater than −0.3 standard deviation resulting in a sample size of 356 pentads. The next step consisted of computing lag composites of U850 anomalies for the active MJO periods. Consistent with the OLR variations, Fig. 6 shows the dipole of easterly (dark shading) and westerly (light shading) wind anomalies propagating eastward. Even though the data records of OLR and U850 are not the same, the composites of OLR and U850 are strongly consistent. For example, when negative OLR anomalies (enhanced convection) are located over the Indian Ocean, the U850 composite indicates westerly and easterly wind anomalies near the enhanced convection. As in the previous case, the composite of the inactive MJO periods simply indicates weak anomalies in the entire equatorial belt (not shown).

Next, we counted the number of extreme events for each grid box and time lag of the composites of U830. Figure 7 summarizes the total counts for each type of extreme event and grid box. The average number is about 56 events for type-I extreme events (Fig. 7a for all grid boxes and lags. As before, a slight preference for more occurrences is observed for lag −2 pentads. The average number of occurrences for type-II cases is about 20, with higher variability between grid boxes and lags (Fig. 7b). The minimum number of occurrences

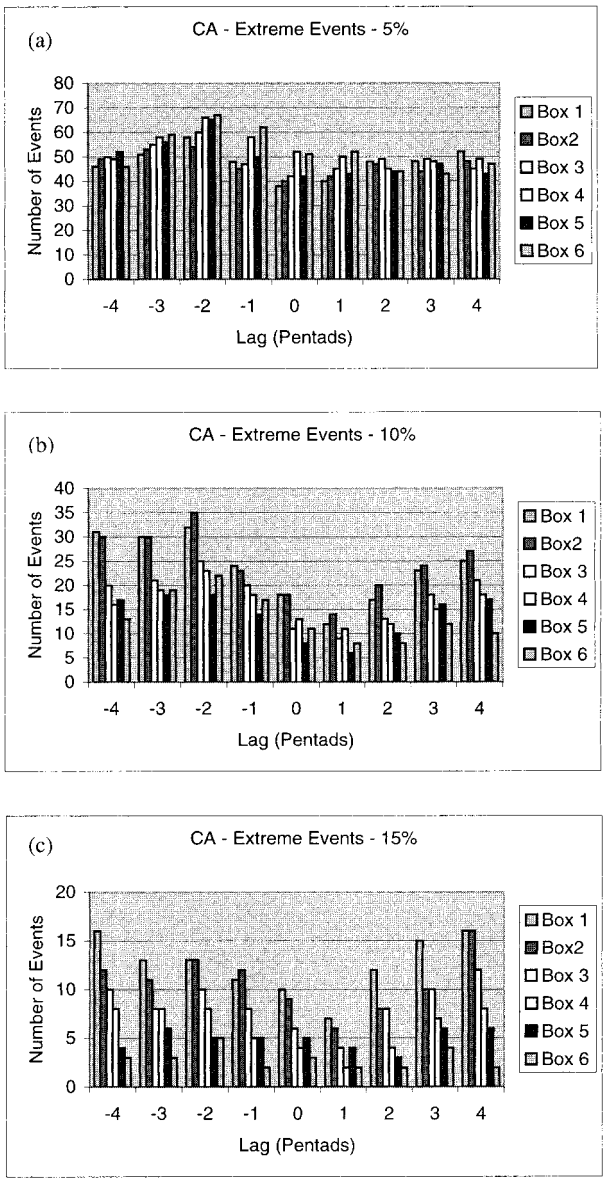

FIG. 7. Total number of extreme events in each of the six grid boxes shown in Fig. 1. The number of occurrences is counted for each lag of the U850 composites illustrated in Fig. 6. Horizontal axes indicate the time lag in pentads. The number of occurrences is counted for extreme events of (a) type I, (b) type II, and (c) type III.

seems to happen for lag +1 pentad. As the threshold increases, Type III (Fig. 7c), the average number of cases is about eight events with even higher differences between the southern and central parts of the state.

The total number of counts for each grid box and type of event during active and inactive MJO periods in the U850 field is summarized in Table 3. The comparison is made with active MJO cases at lag −2 pentads, since there is a slight preference at that phase of the MJO life cycle. The statistical significance, as measured by the *Z* statistic, is also shown. Readily apparent is the much

TABLE 3. Distribution of the number of 5%, 10%, and 15% extreme events for cases of U850 anomalies associated with the MJO (U850 index at lag −2), (sample size $n_1 = 439$ pentads) and no U850 anomalies due to the MJO (sample size $n_2 = 356$ pentads). The value of the Z statistic for each case and box is also indicated. The Z values greater than $Z_{95} = 1.64$ indicate that the difference between the two proportions is significant at 95% confidence level.

	Type-I extreme events (5%)		Type-II extreme events (10%)		Type-III extreme events (15%)	
	Tropical U850 (lag −2)	No tropical U850	Tropical U850 (lag −2)	No tropical U850	Tropical U850 (lag −2)	No tropical U850
Box 1	58	22	32	9	13	6
	$Z = 3.277$		$Z = 3.099$		$Z = 1.220$	
Box 2	54	19	35	11	13	5
	$Z = 3.398$		$Z = 3.001$		$Z = 1.530$	
Box 3	60	22	25	9	10	5
	$Z = 3.447$		$Z = 2.264$		$Z = 0.940$	
Box 4	66	24	23	8	8	2
	$Z = 3.644$		$Z = 2.240$		$Z = 1.661$	
Box 5	65	23	18	6	5	1
	$Z = 3.709$		$Z = 2.055$		$Z = 1.460$	
Box 6	67	26	22	5	5	2
	$Z = 3.440$		$Z = 2.894$		$Z = 0.909$	

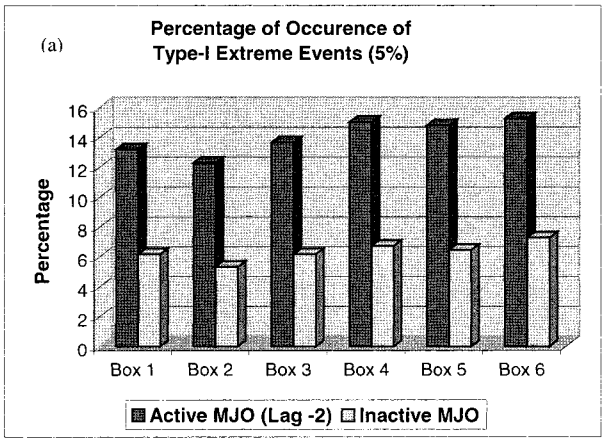

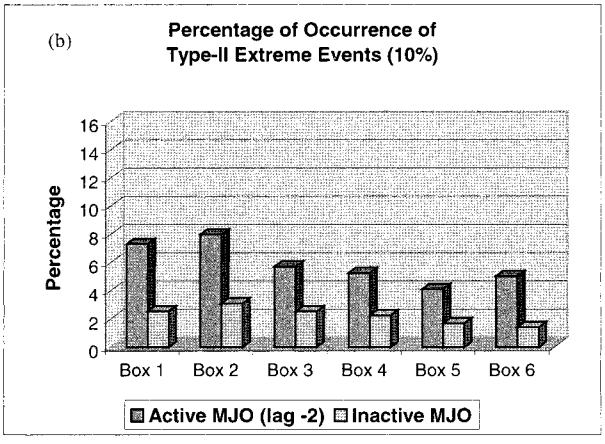

FIG. 8. (a) Percentage of type-I (5%) extreme events that occur during active and inactive MJO periods. (b) Same as in (a), but for type-II (10%) events. Sample sizes are 439 pentads for active MJO and 356 pentads inactive MJO. Percentages are expressed as occurrences from the sample size.

higher number of extreme events during active MJO periods than in inactive ones. The differences in occurrences are statistically significant at 95% level ($Z > 1.64$) for type-I and -II extreme events in all six grid boxes. An important issue to consider in this analysis, however, is how many of the extreme cases occurring during active MJO periods were also coincident with the warm phase of ENSO. We counted the number of extreme events occurring from November to March for the El Niño years of 1957/58, 1965/66, 1968/69, 1972/73, 1982/83, 1986/87, and 1991/92. Only a small fraction of the events shown in Table 3 occurred also during warm ENSO phases. For type-I events the counts were 11, 10, 11, 13, 12, and 14 cases for grid boxes 1–6, whereas for type-II events the counts were 4, 5, 6, 5, 4, and 5. In addition, only one event was reported during the 1965/66 and no extreme events occurred in the 1986/87 El Niño. These results further substantiate the hypothesis that extreme events in California are not only modulated by ENSO but also by tropical intraseasonal activity such as the MJO.

To better illustrate the differences between active and inactive MJO cases and summarize the main results of Table 3, Fig. 8 shows the percentage of occurrences of extreme events of types I and II (number of occurrences divided by the sample size) during active MJO (lag −2 pentads) and inactive periods. While the average percentage of type I for all grid boxes during active MJO periods is 14%, the average for inactive cases is only 6.3%. Likewise, for type II, the average percentages are 5.8% and 2.2% for active and inactive MJO periods, respectively.

5. Interannual variability of the Madden–Julian oscillation and extreme events in California

Since the MJO is known to exhibit significant interannual variations, we now investigate the question of whether or not variations in the amplitude of the oscil-

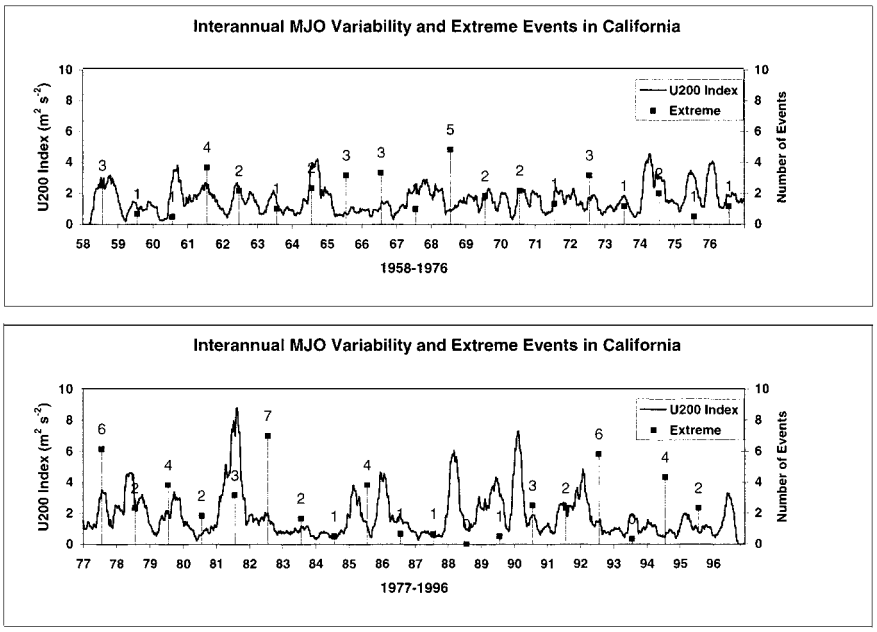

FIG. 9. Interannual variability of the MJO based on U200 index (solid line in units of $m^2\ s^{-2}$, see text for explanation). Also shown is the number of extreme events of Type II averaged over the six grid boxes in California (vertical bars with square and number of occurrences on top of each bar). The number of occurrences was counted from 20–24 Jul in one year to 15–19 Jul of the succeeding year and plotted on 20–24 Jul of each year. Time extends from 1958 to 1996.

lation can be related to high frequency of extreme events on a yearly basis. In this analysis, we consider two indexes to describe interannual variations in the MJO. The first index is similar to the one used by Slingo et al. (1999) in their investigation of the long-term behavior of the MJO, SST, and ENSO. The index uses the zonal component of the wind at 200 hPa (U200), since the activity of the MJO strongly influences the atmospheric angular momentum (Madden and Julian 1994). The bandpassed anomalies (20–90 days) of U200 were first averaged from 10°S to 10°N. We next computed the zonal mean of the equatorial U200 anomalies and raised that quantity to the second power. Then a running mean of 21 pentads (equivalent to 105 days) was applied to that time series resulting in the index that describes the interannual variability of the MJO.

In order to compare the interannual activity of the MJO and variations in precipitation over California, the total number of each type of extreme event (I, II, and III) was counted for each year from 1958 to 1996 and for each gridbox. Because most of the precipitation in central and southern California occurs during the winter season, the number of occurrences was counted from 20–24 July in one year to 15–19 July of the succeeding year.

Figure 9 shows the U200 index from 1958 to 1996. Despite differences in methodology, a close correspondence is observed between our index and the one discussed by Slingo et al. (1999, see their Fig. 7). It is interesting to note the large variations in the amplitude of the U200 index, especially during 1980/81 and the late 1980s and early 1990s. Also displayed in the figure is the number of occurrences of type-II extreme events averaged over the six grid boxes in California. The number of occurrences is plotted on 20–24 July of each year in the period 1958–96. A higher than average number of occurrences are seen during the El Niño years of 1968/69 and 1982/83. Interestingly, very few events occurred during the 1986/87 El Niño. In contrast, the high number of cases during 1977/78 is unrelated to the warm phase of ENSO. We have counted the number of extreme events when the amplitude of the U200 index is above or below one standard deviation, but no large difference is observed between the two situations. In fact, the comparison between the interannual amplitudes of the MJO and the occurrence of extreme events in California does not indicate any obvious relationship. For instance, the high amplitudes during 1981/82 and 1988/89 are not related to high numbers of extreme events.

Since the U200 index described above may not necessarily capture variations that are entirely related to the MJO (Hendon et al. 1999), a second index was constructed based on the zonal components of the wind at 850 hPa (U850). The procedure is identical as before. Anomalies (20–90 days) of U850 were first averaged from 10°S to 10°N. We next computed the zonal mean of the equatorial U850 anomalies and raised it to the second power. A running mean of 21 pentads was applied to that time series resulting in the U850 index. Figure 10 shows the U850 index from 1958 to 1996.

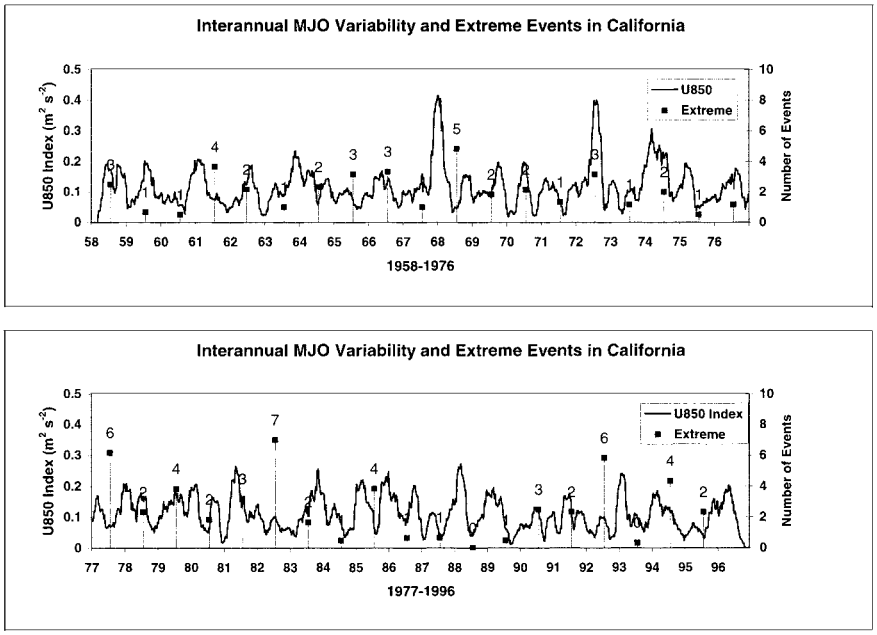

FIG. 10. As in Fig. 9, but based on the U850 index to describe the interannual variability of the MJO (solid line in units of $m^2\ s^{-2}$, see text for explanation).

Also displayed is the number of occurrences of type-II extreme events averaged over the six grid boxes in California (plotted again on 20–24 July of each year). As with the U200 index, these results lead us to infer that high activity of the MJO on interannual timescales is not always connected with high number of extreme events in California.

6. Summary and conclusions

This study investigated the important issue of extreme events in precipitation over the state of California. These events, which occur primarily during the Northern Hemisphere winter season, can bring serious economic losses with great social damages. While most studies have focused on relationships between rainfall in California and the ENSO phenomenon (Cayan et al. 1999), this study showed that systematic and significant relationships exist with tropical intraseasonal activity. The Madden–Julian oscillation, the most distinct mode of tropical intraseasonal variability, seems to modulate the frequency of occurrence of these events as well. Three aspects were investigated. First, the statistical results indicate that the frequency of extreme events are more common when tropical activity associated with the MJO is high, as opposed to periods of quiescent phases of the oscillation. Second, a slight preference for a higher number of events is observed when convective anomalies are located in the Indian Ocean. In this situation, westerly and easterly wind anomalies are observed over the Indian and western Pacific Oceans, respectively. This result is consistent with Mo and Higgins (1998a, b), who showed that the MJO favors wet conditions when enhanced convection is near 150°E. The extreme events seem to happen more frequent, however, when convective anomalies decay to the east of the date line. At this phase of the oscillation, suppressed convection establishes over the western Pacific and new enhanced convection forms again over the Indian Ocean. The third aspect addressed in this study, investigated the interannual variability in the amplitude of the MJO and the occurrence of extreme events over California. Apparently, no direct and systematic relationship between the two is found. This leads us to the important issue of how exactly the MJO interacts with ENSO. During the peak of the warm ENSO phase, when convective activity shifts over the central and eastern Pacific, eastward propagation related to the MJO is not always clear. During these periods, the number of extreme events in California seems to be related to seasonal changes due to ENSO rather than intraseasonal variability associated with the MJO.

The frequency of extreme precipitation events in California is modulated by large-scale circulation patterns from intraseasonal to interannual timescales. The MJO and ENSO phenomenon are the two leading modes of tropical variations modulating these occurrences. Evidently, the occurrence of these extreme events is also largely dictated by baroclinic waves in the midlatitudes of the North Pacific that are unrelated to either MJO or ENSO. Ultimately, what determines high rainfall in any particular location is a combination of factors involving the large-scale, mesoscale, and local features. Recent examples of extreme precipitation to impact the state of

California have been discussed by Masutani and Leetmaa (1999). The months of January and March of 1995 were characterized by active MJO variability as well as high frequency of intense storms that imposed above-average precipitation over most of California. These events also caused extensive property damage and loss of life. Estimates showed over $3 billion in damages and 27 lives claimed by the flooding.

Since the MJO has a slow evolution relative to synoptic weather systems, prediction of the oscillation has the potential to significantly improve extended-range weather forecast in midlatitudes. Until the prediction of the oscillation with numerical weather prediction models is improved (Jones et al. 2000), forecasts provided by statistical models (Waliser et al. 1999) can provide valuable information for local forecasters.

Acknowledgments. This study was funded by a research grant (Contract W-905) from the Water Resources Center, Centers for Water and Wildland Resources, University of California, Riverside. Data support from the National Center for Atmospheric Research (NCAR, which is sponsored by the National Science Foundation) and the National Centers for Environmental Prediction (NCEP) is greatly appreciated. Dr. Wayne Higgins kindly supplied the gridded precipitation data and provided valuable discussions. I am also thankful for the encouragement and support from Professor Catherine Gautier.

REFERENCES

Anderson, T. W., and J. D. Finn, 1996: *The New Statistical Analysis of Data.* Springer–Verlag, 712 pp.

Bryson, R. A., and F. K. Hare, 1974: *Climates of North America.* Vol. 11, *World Survey of Climatology,* Elsevier, 420 pp.

Cayan, D. R., K. T. Redmond, and L. G. Riddle, 1999: ENSO and hydrological extremes in the western United States. *J. Climate,* **12,** 2881–2893.

Chelliah, M., and P. Arkin, 1992: Large-scale interannual variability of monthly outgoing longwave radiation anomalies over the global tropics. *J. Climate,* **5,** 371–389.

Dole, R. M, and N. D. Gordon, 1983: Persistent anomalies of the extratropical Northern Hemisphere wintertime circulation: Geographical distribution and regional persistent characteristics. *Mon. Wea. Rev.,* **111,** 1567–1586.

Duchon, C. E., 1979: Lanczos filter in one and two dimensions. *J. Appl. Meteor.,* **18,** 1016–1022.

Ferranti, L., T. N. Palmer, F. Monteni, and E. Klinker, 1990: Tropical–extratropical interaction associated with the 30–60 day oscillation and its impact on medium and extended range prediction. *J. Atmos. Sci.,* **47,** 2177–2199.

Hendon, H. H., C. Zhang, and J. D. Glick, 1999: Interannual variation of the Madden–Julian Oscillation during austral summer. *J. Climate,* **12,** 2538–2550.

Higgins, R. W., and S. D. Schubert, 1996: Simulations of persistent North Pacific circulation anomalies and interhemispheric teleconnections. *J. Atmos. Sci.,* **53,** 188–207.

——, and K. C. Mo, 1997: Persistent North Pacific circulation anomalies and the tropical intraseasonal oscillation. *J. Climate,* **10,** 223–244.

——, J. E. Janowiak, and Y.-P. Yao, 1996: *A Gridded Hourly Precipitation Data Base for the United States (1963–1993).* National Centers for Environmental Prediction, Climate Prediction Center Atlas 1, 47 pp.

——, Y. Chen, and A. V. Douglas, 1999: Interannual variability of the North American warm season precipitation regime. *J. Climate,* **12,** 653–680.

Horel, J. H., and J. M. Wallace, 1981: Planetary scale atmospheric phenomenon associated with the Southern Oscillation. *Mon. Wea. Rev.,* **109,** 813–829.

Jones, C., and B. C. Weare, 1996: The role of low-level moisture convergence and ocean latent heat fluxes in the Madden and Julian Oscillation: An observational analysis using ISCCP data and ECMWF analyses. *J. Climate,* **9,** 3086–3104.

——, D. E. Waliser, and C. Gautier, 1998: The influence of the Madden–Julian oscillation on ocean surface heat fluxes and sea surface temperature. *J. Climate,* **11,** 1057–1072.

——, ——, J. E. Schemm, and W. K. Lau, 2000: Prediction skill of the Madden and Julian Oscillation in dynamical extended range weather forecasts. *Climate Dyn.,* **16,** 273–289.

Kalnay, E., and Coauthors, 1996: The NCEP/NCAR 40-Year Reanalysis Project. *Bull. Amer. Meteor. Soc.,* **77,** 437–471.

Lau, K. M., and P. H. Chan, 1986: Aspects of the 40–50 day oscillation during the northern summer as inferred from outgoing longwave radiation. *Mon. Wea. Rev.,* **114,** 1354–1367.

Madden, R. A., and P. R. Julian, 1994: Observations of the 40–50-day tropical oscillation—A review. *Mon. Wea. Rev.,* **122,** 814–837.

Maloney, E. D., and D. L. Hartmann, 1998: Frictional moisture convergence in a composite life cycle of the Madden–Julian oscillation. *J. Climate,* **11,** 2387–2403.

Masutani, M., and A. Leetmaa, 1999: Dynamical mechanisms of the 1995 California floods. *J. Climate,* **12,** 3220–3236.

Meehl, G. A., G. N. Kiladis, K. M. Weickmann, M. Wheeler, D. S. Gutzler, and G. P. Compo, 1996: Modulation of equatorial subseasonal convective episodes by tropical–extratropical interaction in the Indian and Pacific Ocean regions. *J. Geophys. Res.,* **101,** 15 033–15 049.

Mitchell, T. P., and W. Blier, 1997: The variability of wintertime precipitation in the region of California. *J. Climate,* **10,** 2261–2276.

Mo, K. C., and R. W. Higgins, 1998a: Tropical influences on California precipitation. *J. Climate,* **11,** 412–430.

——, and ——, 1998b: Tropical convection and precipitation regimes in the western United States. *J. Climate,* **11,** 2404–2423.

Null, J., 1993: Relationships between Type 1 ENSO events and California rainfall, 1949–1991. Preprints, *Eighth Conf. on Applied Climatology,* Anaheim, CA, Amer. Meteor. Soc., 82–88.

Philander, S. G., 1990: *El Niño, La Niña and the Southern Oscillation.* Academic Press, 289 pp.

Raphael, M., and G. Mills, 1996: The role of mid-latitude cyclones in the winter precipitation of California. *Prof. Geogr.,* **48,** 251–262.

Schonher, T., and S. E. Nicholson, 1989: The relationships between California rainfall and ENSO events. *J. Climate,* **2,** 1258–1269.

Slingo, J. M., D. P. Rowell, K. R. Sperber, and F. Nortley, 1999: On the predictability of the interannual behaviour of the Madden–Julian Oscillation and its relationship with El Niño. *Quart. J. Roy. Meteor. Soc.,* **125,** 583–609.

Waliser, D. E., and Zhou, W., 1997: Removing satellite equatorial crossing time biases from the OLR and HRC datasets. *J. Climate,* **10,** 2125–2146.

——, N. E. Graham, and C. Gautier, 1993: Comparison of the highly reflective cloud and outgoing longwave radiation datasets for use in estimating tropical deep convection. *J. Climate,* **6,** 331–353.

——, C. Jones, J. E. Schemm, and N. E. Graham, 1999: A statistical extended-range tropical forecast model based on the slow evolution of the Madden–Julian Oscillation. *J. Climate,* **12,** 1918–1939.

Weickmann, K. M., 1991: El Niño/Southern Oscillation and Madden–Julian (30–60 day) oscillations during 1981–1982. *J. Geophys. Res.,* **96,** 3187–3195.